Journal of Thermal Analysis and Calorimetry, Vol. 75 (2004) 277–291

THERMAL DECOMPOSITION OF HUMBOLDTINE
A high resolution thermogravimetric and hot stage Raman spectroscopic study

R. L. Frost and M. L. Weier*

Inorganic Materials Research Program, Queensland University of Technology, 2 George Street, Brisbane, GPO Box 2434, Queensland 4001, Australia

(Received April 9, 2003; in revised form 6 October 2003)

Abstract

Evidence for the existence of primitive life forms such as lichens and fungi can be based upon the formation of oxalates. These oxalates form as a film like deposit on rocks and other host matrices. Humboldtine as the natural iron(II) oxalate mineral is a classic example. Thermogravimetry coupled to evolved gas mass spectrometry shows dehydration takes place in two steps at 130 and 141°C. Loss of the oxalate as carbon dioxide occurs at 312 and 332°C. Dehydration is readily followed by Raman microscopy in combination with a thermal stage and is observed by the loss of intensity of the OH stretching vibration at 3318 cm^{-1}. The application of infrared emission spectroscopy supports the results of the TG–MS. Three Raman bands are observed at 1470, 1465 and 1432 cm^{-1} attributed the CO symmetric stretching mode. The observation of the three bands supports the concept of multiple iron(II) oxalate phases. The significance of this work rests with the ability of Raman spectroscopy to identify iron(II) oxalate which often occurs as a film on a host rock.

Keywords: high resolution thermogravimetric analysis, hot stage Raman spectroscopy, humboldtine, infrared emission spectroscopy, oxalate

Introduction

The presence of oxalates is widespread in nature. These minerals form as the result of expulsion of heavy metals from fungi, lichens and plants [1–3]. The production of simple organic acids such as oxalic and citric acids has profound implications for metal speciation in biogeochemical cycles [4]. The metal complexing properties of the acids are essential to the nutrition of fungi and lichens and affects the metal stability and mobility in the environment [4]. Lichens and fungi produce the oxalates of heavy metals as a mechanism for the removal of heavy metals from the plant [5]. Humboldtine was identified as a mineral many years ago [6] and its structure was determined [7–9]. Stacking faults in iron(II) oxalates has been determined [10, 11].

* Author for correspondence: E-mail: r.frost@qut.edu.au

1388–6150/2004/ $ 20.00

Akadémiai Kiadó, Budapest
Kluwer Academic Publishers, Dordrecht

Recently Macnish and others identified intracellular calcium oxalate crystals in Geraldton wax flowers (*Chamelaucium uncinatum*). These authors considered that the complexation of the oxalic acid with calcium controlled the concentration of heavy metals in the plant. Importantly the crystals were <1 micron in size and were very difficult to identify using techniques such as X-ray diffraction. Raman spectroscopy however proved useful for the analysis of the calcium oxalate. The presence of these oxalate crystals appears to have an effect similar to that found in cacti [12]. Among the oxalates are the two calcium oxalates known as weddellite (the dihydrate) and whewellite (monohydrate). Ca-oxalate exists in two well-described modifications: as the more stable monoclinic monohydrate whewellite and the less stable tetragonal dihydrate weddellite. Weddellite serves for lichens as a water absorbing and accumulating substrate which transforms to whewellite when humidity drops. Such minerals are important in human physiology as the minerals are found in urinary tracts [13, 14]. Many other divalent oxalates exist in nature. The magnesium based oxalate is known as glushinskite [15, 16]. The copper oxalate is known as moolooite [2, 17] and the iron(II) oxalate as humboldtine [6, 18]. These three oxalates are also the product of lichen growth. Two natural univalent oxalates are known. These are the oxalates of sodium and ammonium known as natroxalate and oxammite [19].

Indeed the presence of oxalates have been evidence for the deterioration of works of art [20–22]. Carbon dating of oxalic acid enables estimates of the age of the works of art [23]. The presence of the oxalates has been used as indicators of climate change [24]. The presence of pigments in ancient works of art effected the growth of lichens on the art works [25]. In calcareous artifacts such as the famous Chinese terra cotta soldiers or Egyptian epigraphs they lead to a destruction of the surface by forming Ca-oxalate layers and thus to a deterioration of the historian work of art. But in places where the surface is covered by some blue colours (Egyptian and Chinese Blue, Chinese Purple) the growth of lichens is inhibited and the artifacts are well preserved. The copper ion contained in the pigments is responsible for this effect since copper is a strong poison for micro-organisms [25]. Weddellite and whewellite very often occur together with gypsum on the surface of calcareous artifacts exposed in the Mediterranean urban environment, as main constituents of reddish patinas called in Italy ‘scialbatura’. The origin of this is a matter of controversy. The observation of the interface between calcite substratum and the above mentioned secondary minerals is an important step in the explanation of alteration process of artifacts of historic and artistic interest [26]. Studies of the black paint has shown the presence of oxalates in the paint with serious implications for remediation [27]. The use of infrared and Raman spectroscopy for the study of oxalates originated with the necessity to study renal stones [28, 29]. FT Raman spectroscopy has been used to study urolithiasis disease that has been studied for many years, and the ethiopathogenesis of stone formation is not well understood [30].

Whilst there have been several studies of synthetic metal oxalates [31–37], few studies of natural oxalates have been forthcoming and few spectroscopic studies of the iron(II) natural oxalate has been undertaken. The objective of this work is to un-

dertake a comparative study using a combination of Raman and infrared spectroscopy combined with a thermal stage [56, 57, 58].

Experimental

Mineral

The humboldtine (sample Number M13748 originated from Bohemia, Czech Republic) was obtained from the Museum Victoria [18]. The sample was phase analyzed using X-ray diffraction and the compositions checked using EDX measurements.

Thermal analysis

Thermal decomposition of the natural oxalate was carried out in a TA® Instruments incorporated high-resolution thermogravimetric analyzer (series Q500) in a flowing nitrogen atmosphere (80 cm^3 min^{-1}). Approximately 50 mg of sample was heated in an open platinum crucible at a rate of 1.0°C min^{-1} up to 500°C. The TG instrument was coupled to a Balzers (Pfeiffer) mass spectrometer for gas analysis. Only selected gases were analyzed.

Raman microprobe spectroscopy

The crystals humboldtine were placed and orientated on the stage of an Olympus BHSM microscope, equipped with 10× and 50× objectives and part of a Renishaw 1000 Raman microscope system, which also includes a monochromator, a filter system and a Charge Coupled Device (CCD). Raman spectra were excited by a HeNe laser (633 nm) at a resolution of 2 cm^{-1} in the range between 100 and 4000 cm^{-1}. Repeated acquisition using the highest magnification was accumulated to improve the signal to noise ratio. Spectra were calibrated using the 520.5 cm^{-1} line of a silicon wafer. In order to ensure that the correct spectra are obtained, the incident excitation radiation was scrambled. Previous studies by the authors provide more details of the experimental technique. Spectra at elevated temperatures were obtained using a Linkam thermal stage (Scientific Instruments Ltd, Waterfield, Surrey, England).

Infrared emission spectroscopy

Details of infrared emission spectroscopy has been previously published [38–40]. Spectroscopic manipulation such as baseline adjustment, smoothing and normalisation were performed using the Spectracalc software package Grams (Galactic Industries Corporation, NH, USA). Band component analysis was undertaken using the Jandel 'Peakfit' software package, which enabled the type of fitting, function to be selected and allows specific parameters to be fixed or varied accordingly. Band fitting was done using a Gauss–Lorentz cross-product function with the minimum number of component bands used for the fitting process. The Gauss–Lorentz ratio was

maintained at values greater than 0.7 and fitting was undertaken until reproducible results were obtained with squared correlations of r^2 greater than 0.995.

Results and discussion

Thermal analysis

The HRTG and MS curves for humboldtine are shown in Figs 1 and 2, respectively. The TG curve for this mineral is complex. Three stages with multiple steps are observed. The first step is observed with two mass losses at 130 and 141°C. The second is a broad step centred upon 235°C. The third stage consists of two mass losses at 312 and 332°C. In harmony with the TG results, mass spectrometry shows the evolved water in two steps at 126 and 132°C. The carbon dioxide is emitted over a broad temperature range commencing at 200°C. Two MS carbon dioxide emission peaks are observed at 322 and 354°C. The values obtained are in agreement with previously published data [41–45].

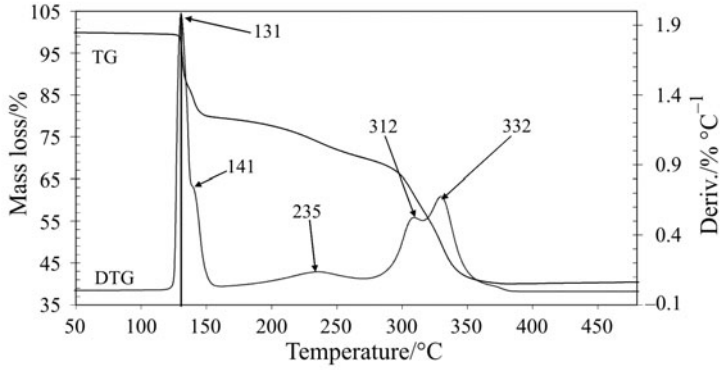

Fig. 1 High resolution thermogravimetric analysis of humboldtine

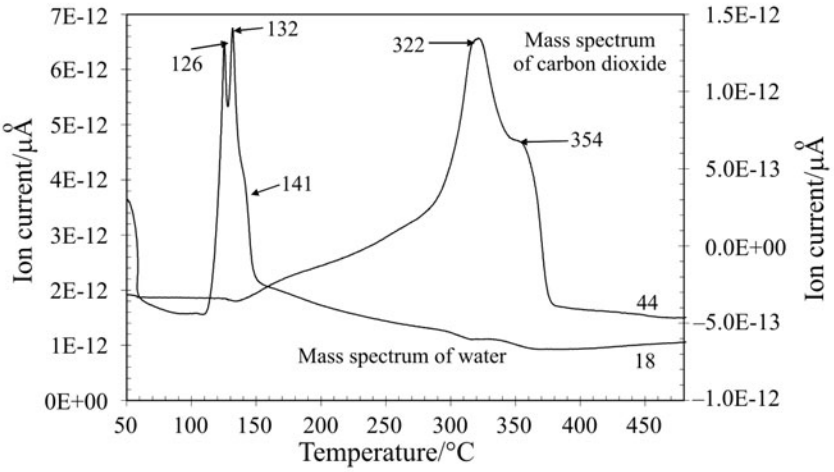

Fig. 2 Mass spectrometric analysis of evolved gases from the thermal treatment of humboldtine

Table 1 Results of the Raman spectral analysis (relative intensity at center) of thermally treated humboldtine

50°C	100°C	150°C	200°C	250°C	300°C	350°C	400°C	450°C
3319 0.118	3325 0.125	3333 0.154						
1709 0.007	1708 0.006	1708 0.004						
1615 0.012	1614 0.010	1613 0.005						
1470 0.154	1469 0.159	1468 0.124						
1465 0.179	1464 0.182	1464 0.209						
1432 0.061	1430 0.061	1429 0.057						
					1580 0.056			
					1382 0.351			
					1326 0.009			
			1297 0.527	1294 0.378		1302 0.398	1301 0.361	1298 0.417
						1254 0.211	1213 0.237	1194 0.129
			1205 0.082	1221 0.111				
			1061 0.068	1057 0.041		1067 0.033	1061 0.025	1061 0.047
983 0.005	980 0.004							
914 0.080	913 0.081	912 0.077						
856 0.004	857 0.003	856 0.002						
			811 0.009					
			652 0.053	653 0.069	690 0.147	672 0.246	662 0.209	656 0.172
			597 0.049	593 0.033			600 0.012	599 0.014
584 0.035	583 0.030	581 0.029						

Table 1 Continued

50°C	100°C	150°C	200°C	250°C	300°C	350°C	400°C	450°C
520 0.050	520 0.117	520 0.085						
			480 0.007	479 0.003	488 0.231			
420 0.004								
			397 0.036	393 0.051		400 0.054	399 0.023	397 0.027
		362 0.001						
					326 0.117			
304 0.003	307 0.005							
288 0.002	285 0.018	291 0.011	285 0.044	281 0.071		289 0.055	287 0.040	286 0.054
					254 0.026			
244 0.040	242 0.051	240 0.117	234 0.015					
				233 0.064			233 0.006	230 0.013
			219 0.011	217 0.046	216 0.011	221 0.023	220 0.011	220 0.016
204 0.074	203 0.053	203 0.059						
		179 0.013		184 0.002				

The proposed mass loss steps are as follows:

$$FeC_2O_4 \cdot 2H_2O \rightarrow FeC_2O_4 \cdot H_2O + H_2O \rightarrow FeC_2O_4 + H_2O$$

$$FeC_2O_4 \rightarrow FeO + CO + CO_2$$

and

$$FeC_2O_4 \rightarrow FeCO_3 + CO$$

$$FeCO_3 \rightarrow FeO + CO_2$$

Based on the HRTG results it is suggested that the iron(II) oxalate looses water in the first stage in steps from the dihydrate to the monohydrate and then to the anhy-

drous compound. It is proposed that the iron(II) oxalate then decomposes in two pathways. The first pathway is the conversion of the iron(II) oxalate to iron(II) oxide and carbon monoxide and carbon dioxide. Berbenni recently studied the reaction of lithium carbonate with ferric oxalate [44]. Such an oxalate was also incorporated into a layer double hydroxide and thermal studies undertaken [46]. Thermal studies of the naturally occurring mineral iron(II) oxalate are less well known. Recently studies have shown valuable information can be obtained by using a combination of thermal analysis and spectroscopic techniques [47–50]. In this work we use a combination of thermogravimetry and hot stage infrared emission and Raman spectroscopy to study the thermal decomposition of the natural mineral humboldtine.

Raman spectroscopy

The Raman spectra of the hydroxyl stretching region thermally treated humboldtine are shown in Fig. 3. The results of the Raman spectroscopic analyses are reported in Table 1. Humboldtine is iron(II) oxalate dihydrate. The spectra clearly show that the intensity of the OH stretching mode is lost at temperatures below 200°C. The band is at 3318 cm^{-1} at 25°C and shifts to 3333 cm^{-1} at 150°C showing a red shift to the band with thermal treatment. The infrared emission spectra shown in Fig. 4 support the Raman data from the thermal treatment of humboldtine. The IE spectra are noisy at the lower temperatures; nevertheless two bands may be identified at 3355 and 3147 cm^{-1}. In the TG experiment two closely overlapping mass loss steps are observed at 131 and 141°C. The MS experiment shows three water vapour evolutions at 126, 132 and 141°C. The results of the Raman and infrared emission spectroscopic studies are in harmony with the TG and MS

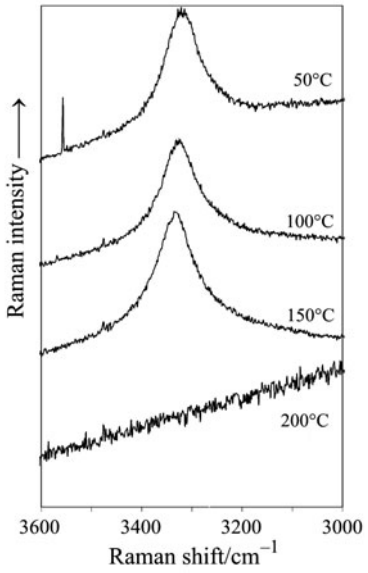

Fig. 3 Raman spectra of the hydroxyl stretching region of thermally treated humboldtine

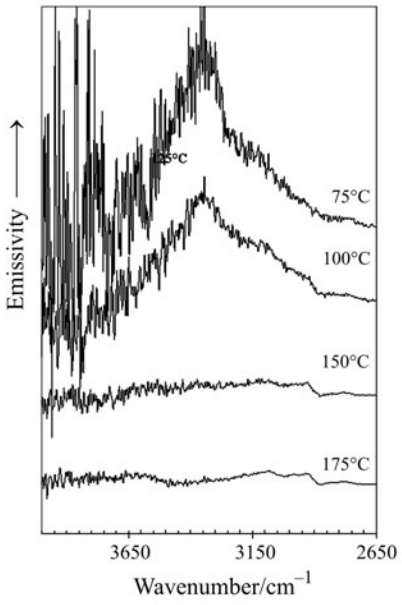

Fig. 4 Infrared emission spectra of the hydroxyl stretching region of thermally treated humboldtine

results in that all four experiments show that there is no water remaining in the structure of the thermally treated humboldtine after 150°C. The TG and MS experiments show at least two mass loss steps. Such steps were not observed in either the Raman or the IES experiment as the temperature intervals between successive spectra were two large. It should be recognised that the band at 3318 cm^{-1} in the Raman spectrum and the band at 3315 cm^{-1} in the infrared emission spectrum are not attributable to the same vibrational mode. The former is ascribed to the OH symmetric stretching vibration and the latter to the OH antisymmetric stretching vibration. Figures 3 and 4 show somewhat conflicting information. The OH bands exist in the Raman spectrum at 150°C; the intensity is low in the infrared emission spectrum at the same temperature. This difference is attributed to the lack of intensity in the infrared emission spectra at low temperatures. It is only at elevated temperatures that sufficient energy enables quality IE spectra to be obtained.

The Raman spectra of the CO stretching region are shown in Fig. 5. Three bands are distinguished in the CO stretching region at 1470, 1465 and 1432 cm^{-1}. These bands are attributed to the CO symmetric stretching vibration. Low intensity bands are observed in the Raman spectra at 1709 and 1615 cm^{-1}. These bands may be attributed to the CO antisymmetric stretching vibration. The intensity of these Raman bands approaches zero by 150°C. If the natural iron(II) oxalate was a single pure chemical then it might be expected that only a single CO stretching mode would be observed. Thermal treatment can cause the conversion of the humboldtine from the dihydrate to the monohydrate and then to the anhydrous iron(II) oxalate. The observation of three CO symmetric stretching vibrations provides credence to the exis-

tence of all three phases. Such a concept of the existence of all three phases is supported by the TG and MS results which show two distinct steps in the dehydration of the humboldtine.

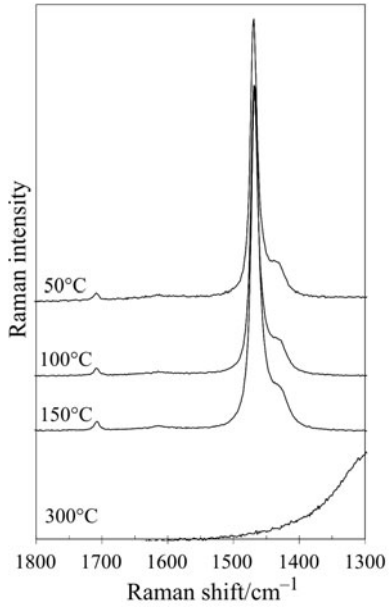

Fig. 5 Raman spectra of the 1300 to 1800 cm^{-1} region of thermally treated humboltine

The IE spectra of the 1100 to 2100 cm^{-1} region of the thermally treated humboldtine are shown in Fig. 6. The results of the infrared emission analyses are reported in Table 2. In the IE spectra at 25, 50 and 75°C, intense bands are observed at 1629 cm^{-1} and no bands are observed at around 1480 cm^{-1}. The band at 1629 cm^{-1} is assigned to the CO antisymmetric stretching vibration. The band at around 1480 cm^{-1} observed at higher temperatures is assigned to the 'forbidden' symmetric stretching vibration. At the lower temperatures the Raman and infrared spectra are mutually exclusive. This mutual exclusion is an indication of a centre of symmetry. Such a centre of symmetry would be achieved if the iron(II) oxalate was planar. Thermal treatment above 100°C results in the loss of the mutual exclusion and hence it is concluded that the iron(II) oxalate is no longer planar but is distorted. It is probable that such distortion arises from stacking faults introduced through thermal treatment [10, 11].

The infrared spectra show quite intense bands centered around 1300 cm^{-1}. These bands may be assigned to B_{3u} OCO stretching mode. The band is observed at 1315 cm^{-1} for aqueous potassium oxalate and at 1313 cm^{-1} for solid potassium oxalate. For weddellite and whewellite bands are observed at 1366 and 1309 cm^{-1}. A band was observed at 1365 cm^{-1} and assigned to the OCO stretching mode for synthetic copper(II) oxalate dihydrate [51, 52]. Humboldtine shows a similar infrared pattern with component bands at 1312 and 1357 cm^{-1}. The IE spectra show intense

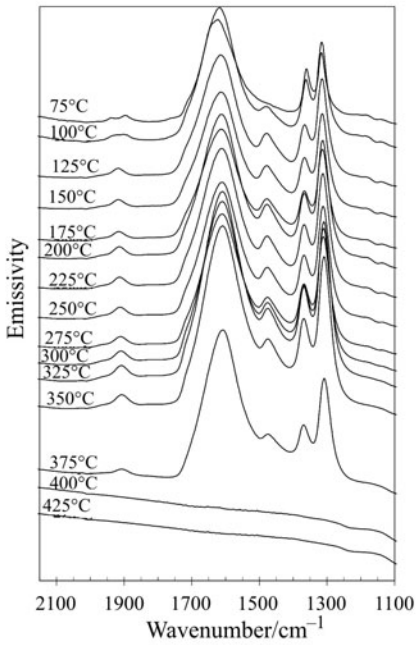

Fig. 6 Infrared emission spectra of the 1300 to 1800 cm^{-1} region of thermally treated humboltine

bands at 1315 cm^{-1} at 75°C which occurs at 1306 cm^{-1} at 375°C before the intensity is lost. A second band is observed at 1360 cm^{-1} and shows an increase in peak position with thermal treatment. The band is observed at 1367 cm^{-1} at 375°C. No bands are observed in these positions in the Raman spectra. It is probable that this latter band is attributable to the B_2 OCO wagging mode. The results of the IE spectra are in harmony with the TG and MS results. IE spectra show that no intensity remains in the characteristic oxalate spectra after 375°C. The TG results show that two mass loss steps are observed at 312 and 332°C. The MS results prove the evolution of carbon dioxide at 322 and 354°C in two mass loss steps. One possible mechanism is that at temperatures above 140°C and below 322°C, the anhydrous iron(II) oxalate is the decomposition product of humboldtine. At 322°C the iron(II) oxalate changes from the bidentate to a mono-dentate ligand and at the second step at 354°C, the mono-dentate oxalate ligand is lost.

The Raman spectra of the C–C stretching region of the thermally treated humboldtine are shown in Fig. 7. The band is observed at 914 cm^{-1} at 75°C and shows a small blue shift with increasing temperature. Only a single C–C stretching vibration is observed. A second low intensity band is observed at 856 cm^{-1} for humboldtine. The band is assigned to the OCO bending mode. A band is not observed in this position for potassium oxalate. The results of the Raman spectra of the thermal treatment of the humboldtine appear to be different from that of either the TG/MS data or the IES data. The loss of the oxalate seems to occur at significantly lower temperatures in the Raman thermal stage than in the IE stage. The infrared emission spectra of the 650

to 1100 cm^{-1} region are shown in Fig. 8. The first observation that can be made is that the C–C stretching mode is either not observed or is only weakly observed in the IE spectra. After thermal treatment of the humboldtine a very low intensity band is observed at around 913 cm^{-1}. It is possible that this is the infrared forbidden C–C stretching vibration. A low intensity band is observed at 943 cm^{-1}. A strong IE band is observed 819 cm^{-1}. The first band shows a strong red shift and the latter a blue shift with thermal treatment (Table 2). These bands are assigned to the OCO bending modes which are strong in the infrared spectrum and of low intensity in the Raman spectra.

Table 2 Results of infrared emission spectral analysis (relative intensity at center) of thermally treated humboldtine

75°C	100°C	125°C	150°C	175°C	200°C	225°C	250°C	275°C
					1965	1962	1963	1962
					0.002	0.001	0.002	0.002
1937	1929	1920	1917	1918	1915	1914	1912	1911
0.003	0.005	0.017	0.004	0.008	0.008	0.007	0.008	0.008
1897	1896							
0.008	0.004							
	1705	1701	1701	1701	1701	1700	1700	1701
	0.011	0.034	0.031	0.028	0.023	0.020	0.016	0.013
1629	1620	1617	1617	1616	1615	1615	1614	1613
0.567	0.641	0.559	0.569	0.565	0.572	0.572	0.575	0.582
1552								
0.150								
	1480	1475	1475	1475	1474	1474	1474	1473
	0.059	0.072	0.069	0.069	0.067	0.060	0.058	0.059
1360	1362	1366	1367	1367	1367	1367	1367	1367
0.056	0.049	0.045	0.045	0.047	0.045	0.048	0.050	0.050
1315	1315	1314	1313	1312	1311	1311	1310	1309
0.124	0.139	0.150	0.156	0.152	0.152	0.160	0.159	0.162
1182	1186	1181	1181	1180	1180	1179	1177	1177
0.002	0.004	0.002	0.002	0.002	0.002	0.002	0.001	0.001
	1133	1134	1133	1132	1131	1131	1130	1131
	0.002	0.001	0.001	0.001	0.001	0.001	0.001	0.001
944	948	948	948	946	945	944	944	942
0.006	0.007	0.009	0.010	0.009	0.010	0.009	0.009	0.007
	913	911	911	910	910	909	909	909
	0.003	0.007	0.008	0.007	0.007	0.007	0.007	0.006
819	813	809	809	809	809	809	809	809
0.054	0.063	0.102	0.103	0.103	0.105	0.107	0.054	0.053
717	716							
0.014	0.004							

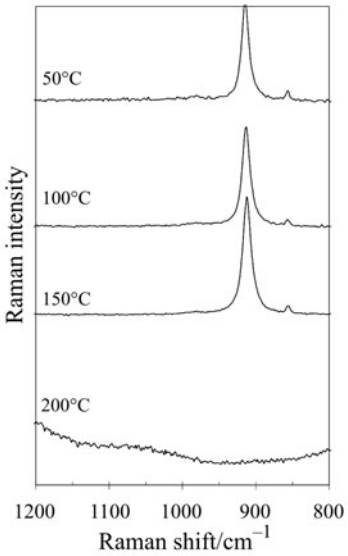

Fig. 7 Raman spectra of the 800 to 1200 cm^{-1} region of thermally treated humboltine

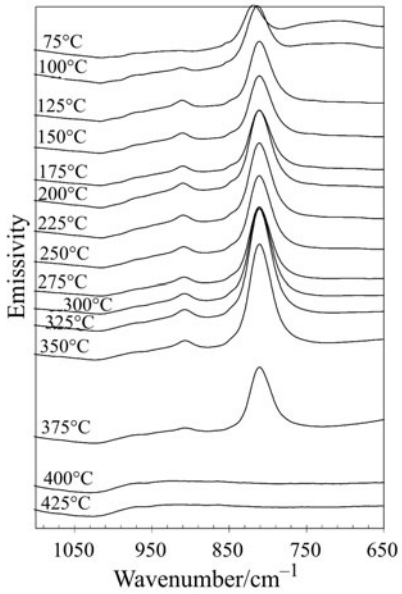

Fig. 8 Infrared emission spectra of the 650 to 1100 cm^{-1} region of thermally treated humboltine

The Raman spectra of the thermally treated humboldtine in the 200 to 700 cm^{-1} region are shown in Fig. 9. The spectra at 50, 100 and 150°C are similar. Above 200°C, the spectra are different and closely resemble the Raman spectrum of hematite. At 25°C, bands are observed at 582 and 518 cm^{-1}. The bands are observed at 584

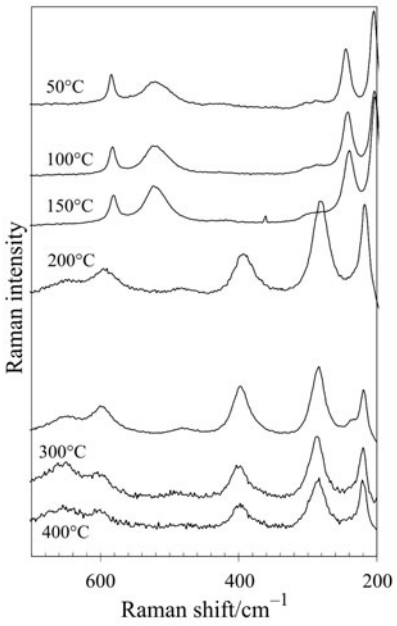

Fig. 9 Raman spectra of the 200 to 700 cm^{-1} region of thermally treated humboltine

and 520 cm^{-1} at 75°C and show a slight blue shift up to 200°C, after which the intensity is lost. Significant changes are observed in the very low wavenumber region of humboldtine before and after 200°C. A set of bands are observed at 204, 244, 288 and 304 cm^{-1}. These bands may be assigned to MO stretching and OMO ring bending modes. At 200°C, bands are observed at 219, 285 and 397 cm^{-1}. These bands correspond to the low wavenumber bands of hematite.

Conclusions

High resolution TG coupled to an evolved gas mass spectrometer shows that dehydration of humboldtine takes place in two stages at around 130 and 141°C. Such two-step dehydration supports the concept of iron(II) oxalate dihydrate changing to iron(II) monohydrate and then to the anhydrous iron(II) oxalate. Such a sequence is supported by the observation of three CO Raman bands. The thermal treatment of iron(II) oxalate was also studied by infrared emission spectroscopy. At low temperatures the infrared and Raman spectra are mutually exclusive; this supports the concept that the iron(II) oxalate is planar. At temperatures above the dehydration temperature this mutual exclusion is lost with the appearance in the infrared emission spectra of a band at 1480 cm^{-1}. The IE spectra strongly support the loss of oxalate over the 275 to 375 temperature range.

If life existed on Mars at some time in the past or even exists in the present time, low life forms such as fungi and lichens may exist. Such organisms may be found in very hostile environments [53–55]. Lichens and fungi can control their heavy metal

intake through expulsion as metal salts such as oxalates. The presence of these oxalates can be used as a marker for the pre-existence of life. Thus the study of the common natural oxalates is of great importance. The minerals on planets such as Mars may be explored by robotic devices which carry portable Raman spectrometers with perhaps fibre optics to collect spectral data. The interpretation of the spectra of natural oxalates is important for these types of studies.

* * *

The financial and infra-structure support of the Queensland University of Technology Inorganic Materials Research Program is gratefully acknowledged. The Australian Research Council (ARC) is thanked for funding Mr Dermot Henry of Museum Victoria.

References

1 H. J. Arnott and M. A. Webb, Scanning Electron Microsc., (1983) 1747.
2 J. E. Chisholm, G. C. Jones and O. W. Purvis, Mineralogical Magazine, 51 (1987) 715.
3 A. Fey-Wyssling, Am. J. Bot., 68 (1981) 130.
4 G. M. Gadd, Mineralogical Soc. Ser., 9 (2000) 57.
5 T. Wadsten and R. Moberg, Lichenologist, 17 (1985) 239.
6 E. Manasse, Rend. Accad. Lincei, 19 (1911) 138.
7 F. Mazzi and C. Garavelli, Periodico mineral, 26 (1957) 269.
8 F. Mazzi and C. L. Garavelli, Periodico mineral, 28 (1959) 243.
9 S. Caric, Bull. Soc. Franc. Mineral Crist., 82 (1959) 50.
10 H. Pezerat, J. Dubernat and J. P. Lagier, Comp. Rend. des Siences de l'Acad. des Sci., Ser. C: Sciences Chimiques, 288 (1968) 1357.
11 J. Dubernat and H. Pezerat, J. Appl. Cryst., 7 (1974) 387.
12 P. V. Monje and E. J. Baran, Plant Phys., 128 (2002) 707.
13 J. P. Pestaner, F. G. Mullick, F. B. Johnson and J. A. Centeno, Arch. Pathology and Lab. Med., 120 (1996) 537.
14 J. Dubernat and H. Pezerat, J. Appl. Cryst., 7 (1974) 387.
15 H. Pezereat, J. Dubernat and J. P. Lagier, C. R. Acad. Sci., Paris, Ser. C, 288 (1968) 1357.
16 M. J. Wilson and P. Bayliss, Mineral. Magazine, 51 (1987) 327.
17 R. M. Clarke and I. R. Williams, Mineral. Magazine, 50 (1986) 295.
18 K. Rezek, J. Sevcu, S. Civis and J. Novotny, Casopis pro Mineralogii a Geologii, 33 (1988) 419.
19 H. Winchell and R. J. Benoit, Am. Mineral., 36 (1951) 590.
20 A. Piterans, D. Indriksone, A. Spricis and A. Actins, Proc. Latvian Acad. of Sci., section. B, Natural, Exact and Applied Sciences, 51 (1997) 254.
21 M. del Monte and C. Sabbioni, Environ. Sci. Technol., 17 (1983) 518.
22 M. del Monte and C. Sabbioni, Sci. Total Environm., 50 (1986) 165.
23 J. Girbal, J. L. Prada, R. Rocabayera and M. Argemi, Radiocarbon, 43 (2001) 637.
24 S. Moore, M. J. Beazley, M. R. McCallum and J. Russ, Preprints of Extended Abstracts presented at the ACS National Meeting, American Chemical Society, Division of Environm. Chemistry, 40 (2000) 4.
25 I. Lamprecht, A. Reller, R. Riesen and H. G. Wiedemann, J. Therm. Anal. Cal., 49 (1997) 1601.
26 R. Alaimo and G. Montana, Neues Jahrbuch fuer Mineralogie, Abhandlungen, 165 (1993) 143.

27 G. Alessandrini, L. Toniolo, F. Cariati, G. Daminelli, S. Polesello, A. Pozzi and A. M. Salvi, Studies in Conservation, 41 (1996) 193.
28 H. Moenke, Chem. Erde, 21 (1961) 239.
29 M. Daudon, M. F. Protat, R. J. Reveillaud and H. Jaeschke-Boyer, Kidney Int., 23 (1983) 842.
30 C. Paluszkiewicz, M. Galka, W. Kwiatek, A. Parczewski and S. Walas, Biospectroscopy, 3 (1997) 403.
31 R. I. Bickley, H. G. M. Edwards and S. J. Rose, J. Molecular Structure, 243 (1991) 341.
32 H. Chang and P. J. Huang, Anal. Chem., 69 (1997) 1485.
33 D. Duval and R. A. Condrate, Sr., Applied Spectroscopy, 42 (1988) 701.
34 H. G. M. Edwards, D. W. Farwell, R. Jenkins and M. R. D. Seaward, J. Raman Spectroscopy, 23 (1992) 185.
35 I. I. Kondilenko, P. A. Korotkov, N. G. Golubeva, V. A. Klimenko and A. I. Pisanskii, Optika i Spektroskopiya, 45 (1978) 819.
36 O. I. Kondratov, E. A. Nikonenko, I. I. Olikov and L. N. Margolin, Zh. Neorg. Khim., 30 (1985) 2579.
37 T. A. Shippey, J. Molecular Structure, 63 (1980) 157.
38 R. L. Frost, Z. Ding, J. T. Kloprogge and W. N. Martens, Thermochim. Acta, 390 (2002) 133.
39 R. L. Frost, Z. Ding, W. N. Martens and T. E. Johnson, Thermochim. Acta, 398 (2003) 167.
40 R. L. Frost, J. Kristóf, E. Horváth and J. T. Kloprogge, J. Raman Spectrosc., 32 (2001) 873.
41 J. Praharaj, S. K. Pati, S. C. Moharana and D. Bhatta, J. Teaching and Res. Chem., 8 (2001) 4.
42 A. V. Shkarin, I. P. Suzdalev, B. M. Kadenatsi and G. M. Zhabrova, Khim. Vys. Energ., 2 (1968) 77.
43 B. S. Randhawa, Thermochim. Acta, 254 (1995) 381.
44 V. Berbenni, A. Marini, G. Bruni and R. Riccardi, Thermochim. Acta, 346 (2000) 115.
45 A. Coetzee, D. J. Eve and M. E. Brown, J. Thermal Anal., 39 (1993) 947.
46 S. Carlino and M. J. Hudson, Solid State Ionics, 110 (1998) 153.
47 E. Horváth, J. Kristóf, R. L. Frost, A. Redey, V. Vágvölgyi and T. Cseh, J. Therm. Anal. Cal., 71 (2003) 707.
48 J. Kristóf, R. L. Frost, J. T. Kloprogge, E. Horváth and E. Makó, J. Therm. Anal. Cal., 69 (2002) 77.
49 J. Kristóf, R. L. Frost, W. N. Martens and E. Horváth, Langmuir, 18 (2002) 1244.
50 J. Kristóf, E. Horváth, R. L. Frost and J. T. Kloprogge, J. Therm. Anal. Cal., 63 (2001) 279.
51 H. G. M. Edwards and P. H. Hardman, J. Molecular Structure, 273 (1992) 73.
52 H. G. M. Edwards and I. R. Lewis, Spectrochim. Acta, Part A.: Molecular and Biomolecular Spectroscopy, 50A (1994) 1891.
53 H. G. M. Edwards, E. M. Newton and J. Russ, J. Molecular Structure, 550–551 (2000) 245.
54 H. G. M. Edwards, N. C. Russell, M. R. D. Seaward and D. Slarke, Spectrochim. Acta, Part A.: Molecular and Biomolecular Spectroscopy, 51A (1995) 2091.
55 H. G. M. Edwards, N. C. Russell and M. R. D. Seaward, Spectrochim. Acta, Part A.: Molecular and Biomolecular Spectroscopy, 53A (1997) 99.
56 E. Horváth, J. Kristóf, R. L. Frost, A. Redey, V. Vágvölgyi and T. Cseh, Hydrazine-hydrate intercalated halloysite under controlled-rate thermal analysis conditions. J. Therm. Anal. Cal., 71 (2003) 707.
57 R. L. Frost, Z. Ding and H. D. Ruan, Thermal analysis of goethite. Relevance to Australian indigenous art. J. Therm. Anal. Cal., 71 (2003) 783.
58 R. L. Frost, W. Martens, Z. Ding and J. T. Kloprogge, DSC and high-resolution TG of synthesized hydrotalcites of Mg and Zn. J. Therm. Anal. Cal., 71 (2003) 429.